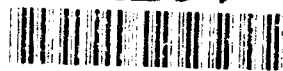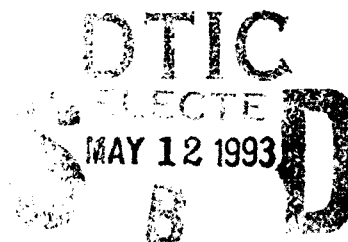AD-A264 111

ARMY RESEARCH LABORATORY

Navier-Stokes Computations for Kinetic Energy Projectiles in Steady Coning Motion - A Predictive Capability for Pitch Damping

Paul Weinacht
Walter B. Sturek

ARL-TR-112   April 1993

DTIC
ELECTE
MAY 12 1993
B

93-10488

93 5 11 15 5

NOTICES

REPORT DOCUMENTATION PAGE

1. AGENCY USE ONLY (Leave blank)	2. REPORT DATE	3. REPORT TYPE AND DATES COVERED
	April 1993	Final, September 1989 - January 1992

4. TITLE AND SUBTITLE

NAVIER-STOKES COMPUTATIONS FOR KINETIC ENERGY PROJECTILES IN STEADY CONING MOTION - A PREDICTIVE CAPABILITY FOR PITCH DAMPING

5. FUNDING NUMBERS

PR: 1L162618AH80
WO: 62618A-00-001 AJ

6. AUTHOR(S)

PAUL WEINACHT   and   WALTER B. STUREK

7. PERFORMING ORGANIZATION NAME(S) AND ADDRESS(ES)

U.S. Army Research Laboratory
ATTN: AMSRL-WT-PB
Aberdeen Proving Ground, MD 21005-5066

8. PERFORMING ORGANIZATION REPORT NUMBER

9. SPONSORING/MONITORING AGENCY NAME(S) AND ADDRESS(ES)

US Army Research Laboratory
ATTN: AMSRL-OP-CI-B (Tech Lib)
Aberdeen Proving Ground, Maryland 21005-5066

10. SPONSORING/MONITORING AGENCY REPORT NUMBER

ARL-TR-112

11. SUPPLEMENTARY NOTES

This report supersedes BRL-IMR-937, March 1990.

12a. DISTRIBUTION/AVAILABILITY STATEMENT

Approved for public release; distribution is unlimited.

12b. DISTRIBUTION CODE

13. ABSTRACT (Maximum 200 words)

Previous theoretical investigations have proposed that the side force and moment acting on a body of revolution in steady coning motion could be related to the pitch-damping force and moment. In the current research effort, this approach has been applied to produce the first known Navier-Stokes predictions of the pitch damping for finned projectiles. The flow field about finned kinetic energy projectiles in steady coning motion has been successfully computed using a parabolized Navier-Stokes computational approach. The computations make use of a rotating coordinate frame in order to solve the steady flow equations. From the computed flow field, the side moment due to coning motion is used to determine the pitch-damping coefficient. The computational predictions of the slope of the side moment coefficient with coning rate normalized by the sine of the angle of attack have been compared with pitch damping coefficients determined from range firings for two finned projectile configurations. The predictions show good agreement with the range data. This computational approach provides a significant predictive capability for the design of kinetic energy projectiles whose terminal ballistic performance can be degraded by moderate levels of yaw at the target.

14. SUBJECT TERMS		15. NUMBER OF PAGES
Projectiles Numerical Analysis Aerodynamic Characteristics Computations Aerodynamics Navier-Stokes Equations		37
		16. PRICE CODE

17. SECURITY CLASSIFICATION OF REPORT	18. SECURITY CLASSIFICATION OF THIS PAGE	19. SECURITY CLASSIFICATION OF ABSTRACT	20. LIMITATION OF ABSTRACT
UNCLASSIFIED	UNCLASSIFIED	UNCLASSIFIED	UL

Intentionally left blank.

TABLE OF CONTENTS

INTENTIONALLY LEFT BLANK.

LIST OF FIGURES

v

Intentionally left blank.

1. INTRODUCTION

Gun-launched kinetic energy (KE) projectiles typically fly with some degree of pitching motion caused by launch disturbances such as the whipping motion of the gun tube, inbore balloting of the projectile, and the sabot discard process. The amplitude of the pitching motion decreases (or damps) as the projectile travels downrange due to the aerodynamic properties of the projectile body. Figure 1 shows the pitching motion of a M735 KE projectile as observed in the BRL Transonic Range and is representative of the motion of finned kinetic energy projectiles. This three-dimensional plot shows the vertical and horizontal components of angle of attack, α and β, as a function of the distance downrange. Two-dimensional projections of the angle of attack components as a function of range are also shown. For this particular shot, launch disturbances produced initial pitch angles of more than six degrees that are subsequently damped during the projectile's flight. For finned KE projectiles, the rate at which the pitching motion is damped is a function of the pitch damping aerodynamic coefficient and the projectile's transverse moment of inertia.

The ability to accurately predict the pitch damping aerodynamic coefficient of KE projectiles is of particular importance to the projectile designer because the terminal ballistic performance of these projectiles is sensitive to the pitch angle at the target. Small pitch angles may result in significant degradation of the penetrator's terminal ballistic performance. Figure 2 shows measurements of terminal ballistic penetration as a function of pitch angle for a long rod penetrator against a laminated armor target at 65 degrees obliquity (Roecker and Grabarek, 1986). Even at small pitch angles, a significant loss of penetration is observed. If the penetrator and the target are closely matched, this degradation of penetrator performance can result in the inability of the penetrator to defeat the target.

Fin stabilized KE projectiles typically do not employ active controls for damping the amplitude of the pitching motion, but rely instead on the aerodynamic properties of the body to produce the necessary pitch damping. A predictive capability for pitch damping assists in the production of projectile designs that will have acceptable levels of pitch at the target. The development of such a predictive capability is the subject of this report.

The pitch damping force and moments are generally produced by the time-dependent motion of the body and, for this reason, are classified as dynamic aerodynamic derivatives. Despite the fact that these coefficients are associated with the time-dependent motion of the projectile, it may be possible to determine the pitch damping coefficients using steady motion. By applying linear flight mechanics theory such as that developed by Murphy (1963), it can be shown that the aerodynamic side force and moment coefficients acting on a projectile in steady coning motion can be related to the pitch damping force and moment coefficients.

1

Steady coning motion is defined as the motion performed by a missile flying at a constant angle with respect to the free stream velocity vector and undergoing a rotation at a constant angular velocity about a line parallel to the freestream velocity vector and coincident with the projectile center of gravity. This is shown schematically in Figure 3. Steady coning motion can be decomposed into constant amplitude sinusoidal pitching motions in the horizontal and vertical planes (Figure 4). Steady coning motion has the advantage of being a steady motion when viewed from the appropriate coordinate frame, while at the same time being composed of pitching motions. The use of steady coning motion to determine the pitch damping aerodynamic coefficients provides an interesting and cost effective approach for determining the aerodynamics that are normally associated with unsteady or time-dependent motions.

Previously, Tobak, Schiff, and Peterson (1969) examined the aerodynamics of bodies of revolution in coning motion and proposed that the non-linear aerodynamic forces and moments acting on a body performing large amplitude non-planar motions could be represented by the aerodynamic forces and moments produced by four characteristic motions: (1) steady angle of attack; (2) pitching motion; (3) rolling motion; and (4) coning motion. Typically, the linear aerodynamic force and moment formulation considers only forces and moments due to the first three motions, and assumes that a non-planar motion can be described by the vector sum of two independent planar motions. The addition of coning motion allows for coupling between planar motions in the non-linear formulation. At small angles of attack where linear variations of the aerodynamic coefficients are expected, their non-linear theory also confirms the linear theory result that the side force and moment due to coning motion are related to the linear pitch damping coefficients.

To provide additional validation for the theory, Schiff and Tobak (1970) performed wind tunnel experiments on a conical body undergoing separate or combined spinning and coning motions. Their experimental results showed good agreement with predictions of the pitch damping force and moment coefficients obtained by using a linearized theory. They also demonstrated that, for their particular geometry and flow conditions, the Magnus force and moment (variation of side force and moment with spin rate and angle of attack) were negligible, thus the linear pitch damping coefficients could be directly determined from the side force and moment due to coning.

Subsequently, Schiff (1972) computed the supersonic inviscid flow about a conical body undergoing coning motion. To compute the flow around the body in coning motion, Schiff utilized a rotating coordinate system. Within the rotating coordinate frame the flow was steady, thus the steady Euler equations could be solved. The governing equations were modified to include the centrifugal and Coriolis force terms. The computed results compared well with experimental results and with estimates of pitch damping coefficients obtained by

2

using a linear theory. Later studies by Agarwal and Rakich (1978), and Lin (1978) also employed rotating coordinate frames to compute the supersonic viscous flow about conical bodies in coning motion.

In this report, pitch damping predictions for finned projectiles are obtained using steady coning motion. The supersonic viscous flow field about these projectiles undergoing coning motion is determined computationally using the parabolized Navier-Stokes technique of Schiff and Steger (1980). The computations are performed in a rotating coordinate frame similar to that employed originally by Schiff (1972). Code modifications required to implement the rotating coordinate frame are discussed. These modifications include the addition of the centrifugal and Coriolis source terms to the governing equations and changes to the shock fitting algorithm. From the computed flow field, the side force and moment due to coning motion are used to determine the pitch damping coefficients. The relation between the side force and moment due to coning and the pitch damping force and moment coefficients is discussed and extensions to the theory required for the analysis of finned projectiles are described. Results are presented for two fielded kinetic energy projectile configurations, the M735 and M829.

2. THEORETICAL BACKGROUND

In this section, the relation between coning motion and pitching motion is first described. Following this description, the relation between the side force and moment due to coning motion and the pitch damping coefficients is developed.

2.1 Relation between Coning and Pitching Motions. As was discussed previously, steady coning motion is defined as the motion performed by a missile flying at a constant angle with respect to the free stream velocity vector (angle of attack) and undergoing a rotation at a constant angular velocity about a line parallel to the freestream velocity vector and coincident with the projectile center of gravity. This is shown schematically in Figure 3. The vertical and horizontal components of the angle of attack, α and β, vary in a periodic fashion as the projectile rotates about the free-stream velocity vector, as shown in Figure 4. The total angle of attack, $\alpha_t \approx \sqrt{\alpha^2 + \beta^2}$ is constant, however.

Both of these components of the angle of attack, when plotted as a function of time, are sinusoidal, constant amplitude, pitching motions that are out of phase with each other by one quarter of a cycle, as shown in Figure 4. By decomposing coning motion in this fashion, it can be observed that coning motion contains a specific linear combination of two

3

orthogonal planar pitching motions.

The term steady coning motion describes the motion of the body about the freestream velocity vector, but does not completely describe the motion of the body. In particular, the projectile may rotate (or spin) about its longitudinal axis. In this report, a particular form of coning motion, *steady lunar coning motion*, is utilized. In steady lunar coning motion, the angular velocity of the projectile results purely from the rotation of the projectile about the freestream velocity vector. This produces a component of angular velocity along the projectile axis, which, by definition, is the spin rate of the projectile. The relation between spin rate, p, and coning rate, $\dot{\phi}$, for the case of steady lunar coning motion is shown below.

$$p = \dot{\phi} \cos \alpha_t = \dot{\phi} \gamma \tag{1}$$

By specifying both the coning rate and the projectile spin rate, the projectile motion is now completely defined. For the particular case of steady lunar coning, the motion can be decomposed into a combination of two orthogonal planar pitching motions, plus a spinning motion at angle of attack.

Planar pitching motion is clearly a time-dependent motion that produces a time-dependent flow field about the projectile. Steady lunar coning motion, on the other hand, will be a steady motion when viewed from a reference frame that is attached to the body (and therefore rotating and translating with the body). In this reference system, no rotation of the pitch plane or the body with respect to the reference frame will be observed. It is important to realize that the steadiness of the motion does not require that the body have special forms of geometric symmetry (i.e. axisymmetry). Furthermore, the flow field generated by steady lunar coning motion is expected to be steady, when viewed from a coordinate frame attached to the body. Steady flow modeling techniques can be applied to determine the flow field due to steady lunar coning motion under the constraints that both the coning rate and the angle of attack are small. (Clearly, the flow may become unsteady at high coning rates or high angles of attack, in much the same way the flow over a body at fixed angle of attack at high incidence can become unsteady due to vortex shedding.) Since the reference frame is a non-inertial system due to the rotation of the coordinate system, the governing equations must be modified. Further details on the implementation of the rotating frame are provided in the discussion of the computational approach.

2.2 Moment Expansion. It is common in aeroballistic applications to utilize a missile-fixed non-rolling coordinate system to describe both the kinematics and the system of forces and moments that act on the projectile in flight (Murphy 1963). The non-rolling coordinate system affords some simplifications, particularly in describing the kinematics.

In this report, the primary reason for initially describing the aerodynamic moments using the non-rolling coordinate system is the fact that the description is well-established. The non-rolling coordinate frame is an orthogonal right-handed system $(\tilde{x}, \tilde{y}, \tilde{z})$ centered at the body center of gravity. The "~" is used to distinguish the non-rolling axis system from the computational coordinate system. The $\tilde{x}$ axis is aligned along the projectile longitudinal axis with the positive direction oriented towards the projectile nose. The $\tilde{z}$ axis is "initially" oriented downward with the $\tilde{x} - \tilde{z}$ plane perpendicular to the ground. The angular motion of the non-rolling coordinate frame is such that the angular velocity of the coordinate frame with respect to an inertial frame is zero in the direction of the $\tilde{x}$ axis. Although the time-dependent orientation of the non-rolling frame may be hard to visualize, the non-rolling frame is essentially equivalent to the "fixed" plane coordinate system for small amplitude motions. In the fixed plane coordinate system, the $\tilde{x} - \tilde{z}$ plane remains perpendicular to the ground for all time. Further details on these coordinate frames can be found in the report by Murphy (1963).

The moment expansion for a finned missile in the non-rolling coordinate frame is shown in Equation 2. This moment expansion is a variant of the expansion discussed by Murphy (1963) for symmetric missiles. The most important difference is that the expression here includes a side moment due to angle of attack, C_{n_α}. The moment formulation uses complex variables to separate the moment components, $\tilde{C}_m$ and $\tilde{C}_n$, that are oriented along the $\tilde{y}$ and $\tilde{z}$ axes, respectively. The third moment component, the roll moment, can be handled separately and is not of consequence in this study.

$$\tilde{C}_m + i\tilde{C}_n = [(\frac{pl}{V})C_{n_{p\alpha}} + C_{n_\alpha} - iC_{m_\alpha}]\tilde{\xi} - \frac{i}{\gamma}[C_{m_q} + \gamma C_{m_\alpha}]\tilde{\xi}' \qquad (2)$$

In the moment expansion, the pitching moment coefficient, C_{m_α}, and pitch damping moment coefficient, $C_{m_q} + C_{m_\alpha}$, produce moments that are proportional to the complex yaw, $\tilde{\xi}$, and yawing rate $\tilde{\xi}'$, respectively. (In the analysis presented here, there is no need to distinguish between pitch and yaw, and the terms may be interchanged. The usage follows that of Murphy (1963).) The Magnus moment coefficient, $C_{n_{p\alpha}}$, accounts for a side moment due to flow asymmetries from a combination of spin and angle of attack.

The side moment due to angle of attack, C_{n_α}, is retained to account for a side moment variation with angle of attack that is caused by the beveled fins. The existence of this side moment was revealed in a previous study (Weinacht and Sturek 1990). The mechanism for this moment can be explained by examining the wind and lee-side fins. The fins, which are beveled to produce roll, may experience different flow on the wind and lee-sides of the body. The lee-side fin may be immersed in the wake created by the body. If the flow is sufficiently different on the wind and lee-sides, the bevels on the wind and lee fins will each produce

a different lift force. The vector sum of the forces on these fins can be non-zero, thereby producing a side moment. Of course, at zero angle of attack, the bevels produce only a roll torque; there is no side moment since the vector sum of the lift produced by the fin bevels is zero.

The moment expansion presented in Equation 2 does not account for variations in the aerodynamic coefficients due to roll orientation. Murphy (1963) has shown that the form of the linear force and moment expansion for a symmetric finned missile with three or more fins should have the same form as for a body of revolution and that the effects of roll orientation are a higher order effect. Computations for finned kinetic energy projectiles have also demonstrated the effect of roll orientation on the aerodynamic coefficients is small (Weinacht and Sturek 1990). In-flight effects of roll orientation are typically not observed because the projectile spin rate is greater than the pitching frequency, causing the effects of roll orientation to be averaged out. Flight bodies with aerodynamic coefficients that exhibit a significant dependence on roll angle may need to be treated with a more general aerodynamic formulation than is presented here (Tobak and Schiff 1975a, 1975b).

2.3 Relation between Side Moment due to Coning and Pitch Damping Moment.

In order to develop the relation between the side moment due to steady lunar coning motion and the pitch damping moment coefficient, it is convenient to resolve the moment components in non-rolling coordinates into moment components that cause rotations in and out of the plane of the angle of attack. This relation is shown below. Here, C_m is the in-plane moment (the moment that causes rotation of the body in the plane of the angle of attack), and C_n is the side moment (the moment that causes rotations of the body out of the angle of attack plane). Also shown are relations for the complex angle of attack, angular rate, and spin rate. These relations, valid for steady lunar coning motion, have been simplified from the general case of arbitrary motion (Levy and Tobak 1970).

$$C_m + iC_n = ie^{-i\gamma\dot\phi t}(\tilde{C}_m + i\tilde{C}_n)$$

$$\tilde\xi = \delta e^{i\gamma\dot\phi t}$$

$$\xi' \equiv \frac{d\tilde\xi}{d(\frac{s}{l})} = i\delta\gamma(\frac{\dot\phi l}{V})e^{i\gamma\dot\phi t}$$

$$p = \gamma\dot\phi \qquad (3)$$

The moment formulation cast in terms of the in-plane and side moments can be written as follows.

$$C_m + iC_n = C_{m_\alpha}\delta + i\{\gamma(\frac{\dot\phi l}{V})C_{n_{p_\alpha}}\delta + C_{n_\alpha}\delta + \delta(\frac{\dot\phi l}{V})[C_{m_q} + \gamma C_{m_{\dot\alpha}}]\} \qquad (4)$$

As expected, the resulting expression for the in-plane and side moments is independent of time. The in-plane moment results only from the pitching moment, while the total side moment consists of contributions from the side moment due to angle of attack, Magnus moment, and pitch damping moment.

Utilizing Equation 4, the variation of side moment with coning rate can be obtained. This relation is valid for linear variations of side moment with coning rate.

$$C_{n_{\dot{\phi}}} \equiv \frac{\partial C_n}{\partial(\frac{\dot{\phi}l}{V})} = \frac{C_n - C_{n_a}\delta}{\frac{\dot{\phi}l}{V}} = \delta(\gamma C_{n_{p\alpha}} + [C_{m_q} + \gamma C_{m_{\dot{\alpha}}}]) \tag{5}$$

The relation of the side moment due to coning, $C_{n_{\dot{\phi}}}$, to the pitch damping moment coefficient, $[C_{m_q} + \gamma C_{m_{\dot{\alpha}}}]$, and the Magnus moment coefficient, $C_{n_{p\alpha}}$, is similar to that presented by Schiff and Tobak (1970) for bodies of revolution. However, for the case of the finned projectiles with beveled or canted fins, the evaluation of $C_{n_{\dot{\phi}}}$ requires that the net side moment, C_n, be determined at two separate coning rates (which may include zero coning rate), due to the presence of a side moment at zero coning rate, $C_{n_a}\delta$. For bodies of revolution, the side moment at a single non-zero coning rate is sufficient to determine the slope, $C_{n_{\dot{\phi}}}$, since the side moment at zero coning rate is zero.

Unfortunately, the pitch damping moment coefficient is not directly related to the side moment due to coning, because of the presence of the Magnus moment term. Furthermore, direct evaluation of the Magnus moment using a Navier-Stokes approach would be difficult and expensive because an unsteady time-accurate calculation is required for non-axisymmetric bodies. However, the Magnus moment coefficient is typically much smaller than the pitch damping coefficient for many projectiles. This has been confirmed by applying simple inviscid theories to estimate the Magnus moment and pitch damping coefficients for finned projectiles similar to those examined in this study (Devan 1989). Additional confirmation can be found from ballistic range testing of kinetic energy projectiles. The Magnus moment coefficient can be quite difficult to measure due in part to its small magnitude in relation to the other aerodynamic coefficients and due to the low spin rates that these projectiles experience in flight.

For the case where the pitch damping moment coefficient is much larger than the Magnus coefficient, Equation 5 can be simplified without a significant loss of accuracy, and the following relation is obtained.

$$[C_{m_q} + C_{m_{\dot{\alpha}}}] \approx \frac{C_{n_{\dot{\phi}}}}{\delta} \tag{6}$$

Because this expression is only valid in the linear aerodynamics regime (small angles of attack), the cosine of the angle of attack, γ, is approximately equal to one and no longer appears in the equation.

A similar expression relating side force due to coning to the pitch damping force and Magnus force can be developed using the same approach as discussed above. Since the Magnus force coefficient is also much smaller than the pitch damping force coefficient, it can be ignored, and the pitch damping force coefficient, $C_{N_q} + C_{N_\alpha}$ can be directly related to the side force coefficient due to coning, C_{Y_ϕ}/δ.

$$[C_{N_q} + C_{N_\alpha}] \approx \frac{C_{Y_\phi}}{\delta} \tag{7}$$

Equations 6 and 7 form the basis for determining the pitch damping force and moment coefficients in this research effort. The side force and moment acting on the projectile due to steady lunar coning motion can be determined by computing the flow field around the projectile and then integrating the pressure and shear stresses acting on the body. Using these two equations, the pitch damping coefficients are obtained from the side force and moment.

3. COMPUTATIONAL APPROACH

Computation of the viscous flow field about the finned projectile configurations was accomplished by solving the thin-layer Navier-Stokes equations using a parabolized Navier-Stokes technique. The computations have been performed in a rotating coordinate frame that is attached to the projectile body and rotates at the coning rate of the projectile. The fluid flow relative to the rotating coordinate frame does not vary with time, allowing the steady (non-time varying) Navier-Stokes equations to be applied. The solution of the steady Navier-Stokes equations can be performed at a reasonable computational cost, typically one and a half to two hours on a Cray-2 or Cray X-MP computer. In order to implement the rotating coordinate frame, the governing equations have been modified to include the effect of centrifugal and Coriolis forces. The steady thin-layer Navier-Stokes equations are shown below.

$$\frac{\partial \hat{E}}{\partial \xi} + \frac{\partial \hat{F}}{\partial \eta} + \frac{\partial \hat{G}}{\partial \zeta} + \hat{H} = \frac{1}{Re} \frac{\partial \hat{S}}{\partial \zeta} \tag{8}$$

Here, $\hat{E}$, $\hat{F}$, and $\hat{G}$ are the inviscid flux vectors, $\hat{S}$ is the viscous flux vector, and $\hat{H}$ is the source term containing the Coriolis and centrifugal force terms that result from the rotating coordinate frame. Each of these matrices are functions of the dependent variables represented by the vector $q^T(\rho, \rho u, \rho v, \rho w, e)$, where ρ and e are the density and the total energy per unit volume, and u, v, and w, are the velocity components in the x, y, and z directions. The flux

terms are defined as follows.

$$\hat{E} = \frac{1}{J}\begin{bmatrix} \rho U \\ \rho u U + \xi_x \mathrm{p} \\ \rho v U \\ \rho w U \\ (e+\mathrm{p})U \end{bmatrix} \qquad \hat{F} = \frac{1}{J}\begin{bmatrix} \rho V \\ \rho u V + \eta_x \mathrm{p} \\ \rho v V + \eta_y \mathrm{p} \\ \rho w V + \eta_z \mathrm{p} \\ (e+\mathrm{p})V \end{bmatrix} \qquad \hat{G} = \frac{1}{J}\begin{bmatrix} \rho W \\ \rho u W + \zeta_x \mathrm{p} \\ \rho v W + \zeta_y \mathrm{p} \\ \rho w W + \zeta_z \mathrm{p} \\ (e+\mathrm{p})W \end{bmatrix}$$

$$\hat{H} = \frac{1}{J}\begin{bmatrix} 0 \\ H_2 \\ H_3 \\ H_4 \\ H_5 \end{bmatrix} \qquad \hat{S} = \frac{1}{J}\begin{bmatrix} 0 \\ m_1\dfrac{\partial u}{\partial\zeta} + m_2\zeta_x \\ m_1\dfrac{\partial v}{\partial\zeta} + m_2\zeta_y \\ m_1\dfrac{\partial w}{\partial\zeta} + m_2\zeta_z \\ m_3 \end{bmatrix} \tag{9}$$

where

$$H_2 = -2\Omega_c\sin\alpha_t\rho v - \rho\Omega_c^2\sin^2\alpha_t(x-x_{cg}) + \rho\Omega_c^2 z\sin\alpha_t\cos\alpha_t$$

$$H_3 = 2\Omega_c\sin\alpha_t\rho u - 2\Omega_c\cos\alpha_t\rho w - \rho\Omega_c^2 y\sin^2\alpha_t - \rho\Omega_c^2 y\cos^2\alpha_t$$

$$H_4 = 2\Omega_c\cos\alpha_t\rho v + \rho\Omega_c^2\sin\alpha_t\cos\alpha_t(x-x_{cg}) - \rho\Omega_c^2 z\cos^2\alpha_t$$

$$\begin{aligned} H_5 = &(-\Omega_c^2\sin^2\alpha_t(x-x_{cg}) + \Omega_c^2 z\sin\alpha_t\cos\alpha_t)\rho u - (\Omega_c^2 y\sin^2\alpha_t + \Omega_c^2 y\cos^2\alpha_t)\rho v \\ &+(\Omega_c^2\sin\alpha_t\cos\alpha_t(x-x_{cg}) - \Omega_c^2 z\cos^2\alpha_t)\rho w \end{aligned} \tag{10}$$

$$\begin{aligned} U &= u\xi_x \\ V &= u\eta_x + v\eta_y + w\eta_z \\ W &= u\zeta_x + v\zeta_y + w\zeta_z \end{aligned} \tag{11}$$

$$\begin{aligned} m_1 &= (\mu + \mu_t)(\zeta_x^2 + \zeta_y^2 + \zeta_z^2) \\ m_2 &= \frac{1}{3}(\mu + \mu_t)(\zeta_x\frac{\partial u}{\partial\zeta} + \zeta_y\frac{\partial v}{\partial\zeta} + \zeta_z\frac{\partial w}{\partial\zeta}) \\ m_3 &= \frac{1}{(\gamma-1)}(\frac{\mu}{Pr} + \frac{\mu_t}{Pr_t})(\zeta_x^2 + \zeta_y^2 + \zeta_z^2)\frac{\partial a^2}{\partial\zeta} + \frac{1}{2}m_1\frac{\partial q^2}{\partial\zeta} \\ &\quad + m_2(u\zeta_x + v\zeta_y + w\zeta_z) \end{aligned} \tag{12}$$

$$a^2 = \frac{\gamma\mathrm{p}}{\rho} \tag{13}$$

$$q^2 = u^2 + v^2 + w^2 \tag{14}$$

$$\begin{aligned} &\xi_x = 1/x_\xi \\ &\eta_x = J(z_\xi y_\zeta - y_\xi z_\zeta) \qquad \eta_y = J(x_\xi z_\zeta) \qquad \eta_z = J(-x_\xi y_\zeta) \\ &\zeta_x = J(y_\xi z_\eta - z_\xi y_\eta) \qquad \zeta_y = J(-x_\xi z_\eta) \quad \zeta_z = J(x_\zeta y_\eta) \\ &J = 1/\left(x_\xi(y_\eta z_\zeta - y_\zeta z_\eta)\right) \end{aligned} \tag{15}$$

9

The form of the source terms, H_2, H_3, H_4, H_5, assumes that the x-axis is oriented along the projectile's longitudinal axis and the $x - z$ plane is in the pitch-plane.

The pressure, p, can be related to the dependent variables by applying the ideal gas law.

$$p = (\gamma - 1)\left[e - \frac{\rho}{2}q^2\right] \tag{16}$$

The turbulent viscosity, μ_t, which appears in the viscous matrices, is computed using the turbulence model of Baldwin and Lomax (1978).

The thin-layer equations are solved using the parabolized Navier-Stokes technique of Schiff and Steger (1980). Following the approach of Schiff and Steger, the governing equations, which have been modified here to include the Coriolis and centrifugal force terms, are solved using a conservative, approximately factored, implicit finite-difference numerical algorithm as formulated by Beam and Warming (1978). The equations are first linearized and placed in delta form, where the equations are solved for the difference in the dependent variables rather than the variables themselves. This set of equations is then factored using the approach of Beam and Warming. The following set of equations is obtained.

$$\left[\tilde{A}_s^j + (1 - \alpha)\Delta\xi\left(\delta_\eta \check{B}^j + \check{D}^j\right)\right]\Delta\tilde{q}^* = RHS \tag{17}$$

$$\left[\tilde{A}^j + (1 - \alpha)\Delta\xi\left(\delta_\zeta \check{C}^j - \frac{1}{Re}\left(\bar{\delta}_\zeta \check{M}^j\right)\right)\right]\Delta\tilde{q}^j = \tilde{A}_s^j\Delta\tilde{q}^* \tag{18}$$

$$
\begin{aligned}
RHS = & -(\tilde{A}_s^j - \tilde{A}_s^{j-1})\tilde{q}^j + \alpha(\hat{E}_s^j - \hat{E}_s^{j-1}) - \left[(\xi_x/J)^{j+1}E_p^j - (\xi_x/J)^j E_p^{j-1}\right] \\
& -(1 - \alpha)\Delta\xi\{\delta_\eta\left[\eta_x^{j+1}(E/J)^j + \eta_y^{j+1}(F/J)^j + \eta_z^{j+1}(G/J)^j\right] \\
& +\delta_\zeta\left[\zeta_x^{j+1}(E/J)^j + \zeta_y^{j+1}(F/J)^j + \zeta_z^{j+1}(G/J)^j\right] \\
& +\hat{H}^j - \frac{1}{Re}\bar{\delta}_\zeta\hat{S}^j + \Phi\}
\end{aligned}
\tag{19}
$$

The form of the equations, as well as the notation, is similar to that used by Schiff and Steger. Here, $\tilde{A}$, $\check{B}$, $\check{C}$, and $\check{M}$ are the Jacobian matrices of the flux vectors $\hat{E}$, $\hat{F}$, $\hat{G}$, and $\hat{S}$. Further details on the definitions of these matrices can be found in the paper of Schiff and Steger (1980). The important difference in the current formulation is the addition of the matrices $\check{D}$ and $\hat{H}$ due to the rotating coordinate system. Although the Jacobian matrix of the source term, $\check{D}$, can be included in either the circumferential inversion or in the normal inversion, including this term in the circumferential inversion simplifies slightly the implementation of the shock fitting boundary conditions.

The computations presented here were performed using a shock fitting procedure reported by Rai and Chaussee (1983). This procedure solves the five Rankine-Hugoniot jump conditions, two geometric shock-propagation conditions, and one compatibility equation to

determine the values of the five dependent variables immediately downstream of the shock, as well as the position of the shock. By including the implicit part of the source term due to the rotating coordinate frame in the circumferential inversion, the shock fitting procedure of Rai and Chaussee can be used without modification as long as the correct free-stream conditions are specified. The freestream values of the dependent variables are shown below in non-dimensional form.

$$\rho = 1$$
$$\rho u = M_\infty \cos \alpha_t + y\Omega_c \sin \alpha_t$$
$$\rho v = \Omega_c(z \cos \alpha_t - (x - x_{cg}) \sin \alpha_t)$$
$$\rho w = M_\infty \sin \alpha_t - y\Omega_c \cos \alpha_t$$
$$e = p_\infty/(\gamma - 1) + \frac{1}{2}\{(M_\infty \cos \alpha_t + y\Omega_c \sin \alpha_t)^2$$
$$+(\Omega_c(z \cos \alpha_t - (x - x_{cg}) \sin \alpha_t))^2 + (M_\infty \sin \alpha_t - y\Omega_c \cos \alpha_t)^2\} \qquad (20)$$

The computational results presented here were obtained using a grid that consisted of 60 points between the body and the bow shock. Due to a lack of circumferential symmetry, gridding was performed around the entire circumference of the body. Over the forebody, 72 circumferential points were used. Grid resolution was increased to 300 points on the fin hub. The grid over the finned portion of the body was generated using an elliptic grid generation scheme presented by Rai, Chaussee, and Rizk (1983). On the axisymmetric part of the body, about 50 marching (axial) planes were required for each caliber of body length. Axial grid resolution was doubled over the finned portion of the body.

4. RESULTS

Computations have been performed to determine the aerodynamics of kinetic energy projectiles in steady lunar coning motion. Results have been obtained for two fielded kinetic energy projectiles: the M735 and the M829. Schematics of these projectiles, including details of the fin geometry, are shown in Figures 5-10. The fins on both of these projectiles have roll-producing beveled surfaces at the leading and trailing edges of the fins. Particular care has been taken to model the fin geometry accurately. It should be noted that the fins on the M829 projectile overhang the base. This aspect of the projectile was modeled by extending the base so that it was aligned with the trailing edge of the fin blades. This allowed the flow field to be computed up to the trailing edge of the fins. However, when the pressure and viscous stresses were integrated to compute the forces acting on the body, the contribution from this part of the body was not considered. Because the flow is supersonic and the fins

are not immersed in the recirculating flow in the base, the flow field adjacent to this region can be considered to be reasonably well modeled. Though not shown, the cylindrical portion of these bodies have a number of circumferential grooves which cover nearly two-thirds of the body. The effect of these grooves is not modeled in the current computations, though it is a subject of current research.

The computations have been performed over a range of Mach numbers ($M_\infty = 3.0$ to 5.5), coning rates ($\dot\phi D/V = 0.0$ to 0.010), and angles of attack ($\alpha_t = 1°$ to $5°$) for free-flight, sea-level atmospheric conditions. The variation of the side force and moment with coning rate normalized by the angle of attack has been used to determine the pitch damping coefficients for these finned projectiles. Comparisons are made with data obtained from range firings (Brandon). The results for each projectile are discussed separately in the following two sections.

4.1   M735 Projectile. The computed variation of the side moment coefficient with coning rate at Mach 4 and two degrees angle of attack is shown in Figure 11. The variation of the side moment coefficient with coning rate is seen to be linear across the range of coning rates examined here. This range of coning rates is representative of the pitching frequencies experienced by the M735 projectile in flight. At Mach 4, the non-dimensional pitching frequency of the projectile is 0.004, where the form of the non-dimensionalization is the same as for the coning rate. The results also show the existence of a small non-zero side moment coefficient at zero coning rate. As discussed previously, this side moment is due to bevels on the fins (Weinacht and Sturek 1990). The existence of this side moment at zero coning rate requires that computations be performed for at least two coning rates in order to evaluate the variation of the side moment coefficient with coning rate, C_{n_ϕ}.

Figure 12 shows C_{n_ϕ} as a function of δ (the sine of the angle of attack) at Mach 4. The dashed line displayed on this figure is representative of a linear variation of C_{n_ϕ} with δ across the range of angles of attack examined. The computed results show that, at small angles of attack, C_{n_ϕ} varies linearly with δ, but departs from a linear variation as the angle of attack increases.

Figure 13 shows the development of C_{n_ϕ}/δ over the M735 kinetic energy projectile at Mach 4 and two degrees angle of attack. As discussed previously, C_{n_ϕ}/δ should be a reasonable representation of the pitch damping coefficient, $C_{m_q} + C_{m_\alpha}$, in the linear aerodynamic regime. This figure shows that the fins contribute most of the side moment due to coning (and hence, the pitch damping) with a smaller contribution from the nose.

The Mach variation of $C_{m_q} + C_{m_\alpha}$ for the M735, as determined from C_{n_ϕ}/δ, is shown

in Figure 14. The computed results are compared with range measurements of the pitch damping coefficient. Though the range data shown here are considered well-determined, some scatter is still evident because damping rates are typically difficult to measure. The experimental results do reflect the expected level of accuracy in determining this coefficient experimentally. The comparisons show that the computational results are within the accuracy of the experimental data and provide a measure of validation of the computational approach.

The predicted variation of the damping force, $C_{N_q} + C_{N_{\dot{\alpha}}}$, as a function of Mach number is shown in Figure 15. This coefficient was determined from the variation of the side force coefficient with coning rate, C_{Y_ϕ}/δ. The pitch damping force coefficient appears in the swerve equation (the equation that describes in-flight motion of the projectile center of gravity). For finned projectiles, the fluctuating component of the swerving motion is composed of contributions from the lift and pitch damping force. The fluctuating component of the swerving motion for a damped planar pitching motion is shown in Figure 16. The relative contributions from the lift and pitch damping forces are also shown. The contribution from the pitch damping force coefficient is seen to be a relatively small portion of the motion, despite the large magnitude of the coefficient itself. Because of this, it is very poorly determined from range firings, thus no experimental data is shown. This coefficient is, however, required for determining the change in the pitch damping moment coefficient due to changes in center of gravity location. Thus, the ability to predict the pitch damping force coefficient is still a significant result.

4.2 M829 Projectile. Similar computations were performed for the M829 kinetic energy projectile. Figure 17 shows the predicted variation of the pitch damping moment coefficient with Mach number for the M829. Again, the computed results are compared with range measurements. The range data has considerable scatter because the total angle of attack experienced by the projectiles during the range firings was very small (typically less than one degree). Thus, the rate at which the amplitude of the pitching motion decreased in flight was difficult to determine. The computational results are within the scatter of the range data. Both the computations and the range results show the order of magnitude increase in the coefficient compared with the predictions shown for the M735. This increase is primarily due to the larger length-to-diameter ratio (L/D) of the M829 (L/D $\approx$ 23) compared with the M735 (L/D $\approx$ 14). The predicted variation of the pitch damping force coefficient as a function of Mach number is shown in Figure 18. Again, no range data are shown because this coefficient is poorly determined. This coefficient is, however, useful for determining the variation of the pitch damping moment coefficient with changes in center of gravity position.

13

One situation where changes in the center of gravity location are often encountered is in aerodynamic range testing of kinetic energy projectiles. Because of restrictions on firing kinetic energy projectiles with heavy metal penetrators through aerodynamic test ranges, surrogate projectiles are often used. Externally, these projectiles appear the same as the fielded round, though the internal heavy metal core has been replaced with a steel core. Replacing the penetrator core can result in a shift in the center of gravity. In the case of the M829, this shift is greater than a quarter of a caliber.

The effect of center of gravity (CG) shift on the damping coefficients was investigated in two ways. First, flow field computations were performed to determined the effect of CG location on the side force and moment due to coning (and hence on the pitch damping force and moment coefficients). Since the projectile rotates about the CG position, the approach involved separate flow field calculations for each CG position. The CG position was moved fore and aft of the baseline CG position by 1 and 2 body diameters. These results are displayed in Table 1 for Mach numbers of 3, 4, and 5. The pitch damping moment becomes more negative (indicative of stronger damping) as the CG position moves forward.

Table 1. CG Translation - Comparison of Results Using CG Translation Equations and Direct Computation

MACH NUMBER	s_{cg}	COMPUTED		TRANSLATED	
		C_{Y_ϕ}/δ	C_{n_ϕ}/δ	C_{Y_ϕ}/δ	C_{n_ϕ}/δ
3.0	-2.0	224.37	-1550.1	224.61	-1551.2
	-1.0	241.89	-1853.2	242.01	-1853.9
	+1.0	276.93	-2564.6	276.81	-2563.7
	+2.0	294.45	-2972.8	294.21	-2970.8
4.0	-2.0	179.59	-1373.4	179.85	-1374.9
	-1.0	195.32	-1615.7	195.45	-1616.6
	+1.0	226.78	-2194.7	226.65	-2193.6
	+2.0	242.52	-2531.5	242.25	-2528.9
5.0	-2.0	136.80	-1177.2	137.08	-1178.8
	-1.0	150.78	-1361.1	150.92	-1362.0
	+1.0	178.75	-1812.7	178.62	-1811.5
	+2.0	192.75	-2080.6	192.46	-2077.8

As an alternative to the first approach, the effect of CG position on the pitch damping force and moment coefficients can be determined using the center of gravity translation relations presented by Murphy (1963). The relations, presented by Murphy for the individual

aerodynamic coefficients, are combined to obtain relations for the coefficients of interest here. These relations for the pitch damping and Magnus force and moments are shown below. The coefficients on the left-hand side of the equations (denoted with a "^") represent the predicted value for a CG shift of s_{cg} body diameters. The aerodynamic coefficients on the right side of these expressions represent the values for the baseline configuration.

$$
\begin{aligned}
\hat{C}_{N_q} + \hat{C}_{N_\alpha} &= C_{N_q} + C_{N_\alpha} + s_{cg}C_{N_\alpha} \\
\hat{C}_{m_q} + \hat{C}_{m_\alpha} &= C_{m_q} + C_{m_\alpha} - s_{cg}(C_{N_q} + C_{N_\alpha}) + s_{cg}C_{m_\alpha} - s_{cg}^2 C_{N_\alpha} \quad (21) \\
\hat{C}_{Y_{p\alpha}} &= C_{Y_{p\alpha}} \\
\hat{C}_{n_{p\alpha}} &= C_{n_{p\alpha}} - s_{cg}C_{Y_{p\alpha}}
\end{aligned}
$$

Since the pitch damping force and moment coefficients are related to the side force and moment due to coning, (Equations 6 and 7), the side force and moment coefficients due to coning exhibit the same variation with CG position.

$$
\begin{aligned}
\hat{C}_{Y_\phi}/\delta &= C_{Y_\phi}/\delta + s_{cg}C_{N_\alpha} \quad (22) \\
\hat{C}_{n_\phi}/\delta &= C_{n_\phi}/\delta - s_{cg}(C_{Y_\phi}/\delta) + s_{cg}C_{m_\alpha} - s_{cg}^2 C_{N_\alpha}
\end{aligned}
$$

The derivation of these relations does not require that the Magnus force and moment be neglected. The effect of the Magnus coefficients is simply absorbed into the coefficients C_{Y_ϕ} and C_{n_ϕ}, and adds no additional terms to the right-hand side of these equations.

Using these relations and the aerodynamic coefficient predictions for the baseline configuration, predictions of the side force and moment variation due to coning for varying CG position were obtained. These results are included in Table 1. The differences between the direct computation of the side moment coefficient at the various CG locations and the values obtained from the CG translation relations is less than 0.2%, and provides additional validation of the computational approach. The side moment (and hence the pitch damping) varies by more than ± 35% for a center of gravity shift of ±2 calibers. Changing the CG position is one possible approach for increasing or decreasing the pitch damping of these projectiles.

5. CONCLUSION

The flow field about finned kinetic energy projectiles in steady coning motion has been successfully computed using a parabolized Navier-Stokes computational approach. The computations make use of a rotating coordinate frame. Relative to this coordinate frame, the flow does not vary with time, allowing the steady flow equations to be solved. Using linear flight mechanics theory, the side moment due to coning is related to the pitch damping and Magnus moment coefficients. For small Magnus moment coefficients, the pitch damping

coefficient is directly proportional to the side moment due to coning. The computational results show that the side moment due to coning varies linearly with coning rate over a range of coning rates that encompasses the pitching frequency of the projectile. For constant coning rate, the side moment coefficient also shows a linear behavior with the sine of the angle of attack up to about two degrees angle of attack, and deviates slightly from the linear behavior at higher angles of attack. The computational predictions of the slope of the side moment coefficient with coning rate normalized by the sine of the angle of attack have been compared with pitch damping coefficients determined from range firings. For the M735 kinetic energy projectile, the predictions are in good agreement with the range data. The computational results for the M829 are within the scatter of the range data. Both the computational predictions and the range data for the M829 show a substantial increase in the pitch damping coefficient when compared to the damping of the M735. This is primarily due to the larger length-to-diameter ratio of the M829.

The favorable comparisons with range data and the efficiency of the computational approach demonstrate the utility of this newly developed capability. To date, several advanced kinetic energy projectile concepts have been examined using this capability.
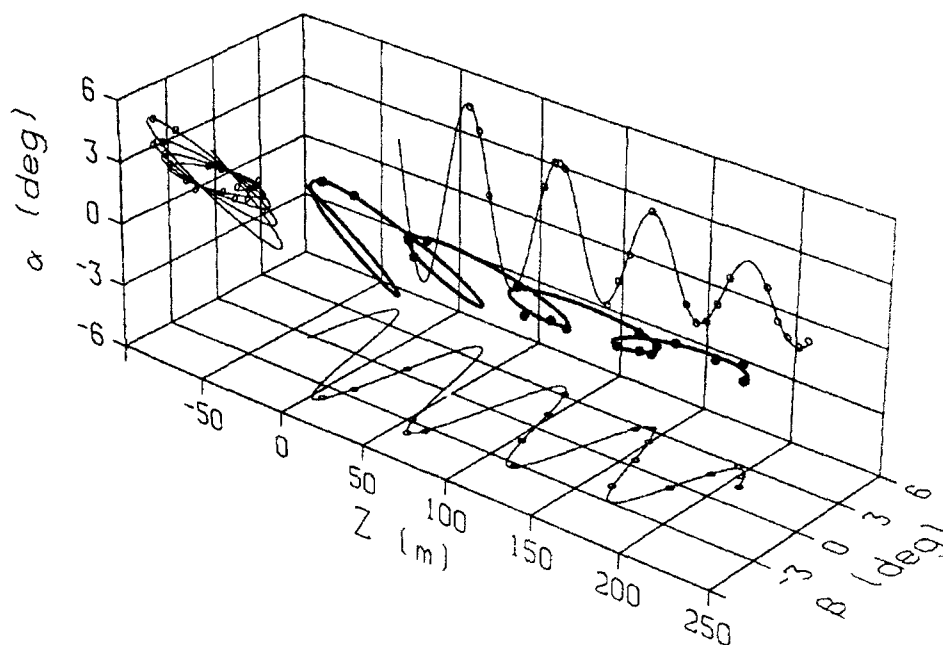
Figure 1. Pitching motion of M735 KE projectile - Round 16423.
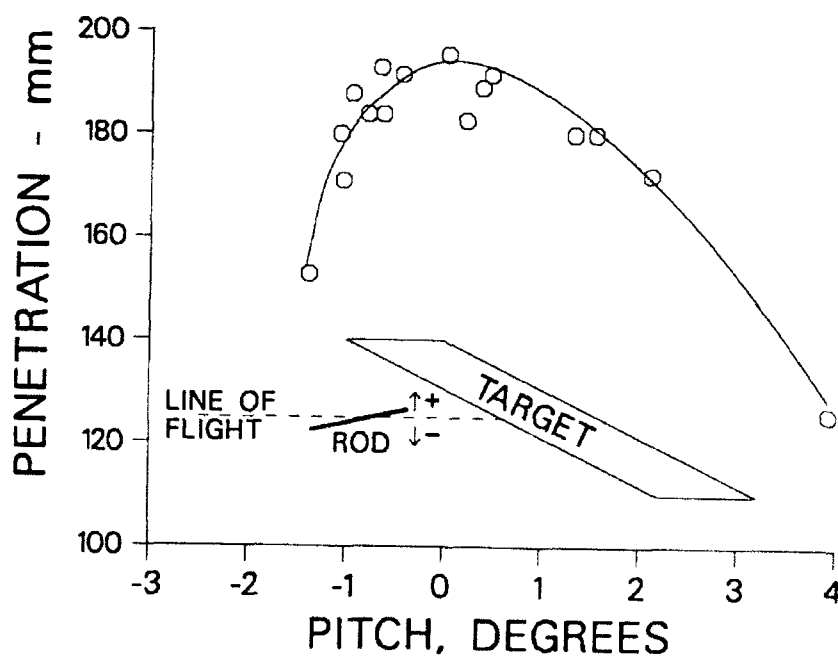
Figure 2. Penetration as a function of pitch angle, 65 degree obliquity target.

17
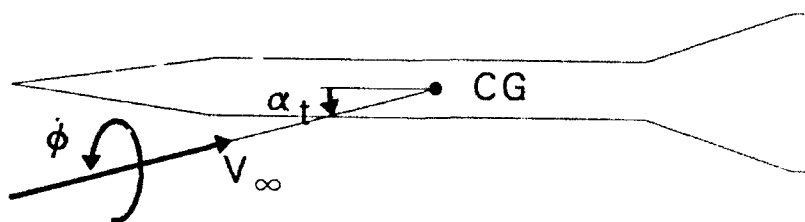
Figure 3. Schematic of coning motion.
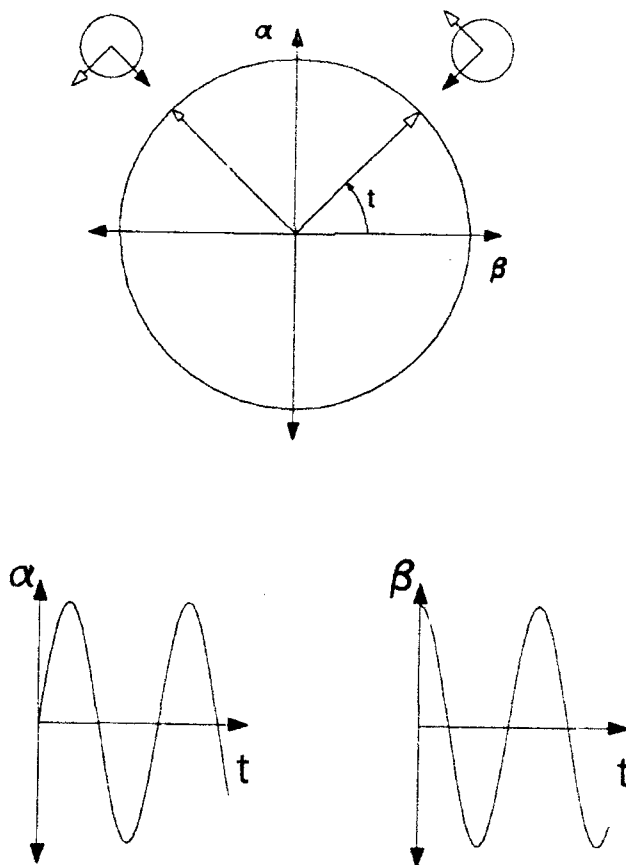
Figure 4. Components of coning motion.

18
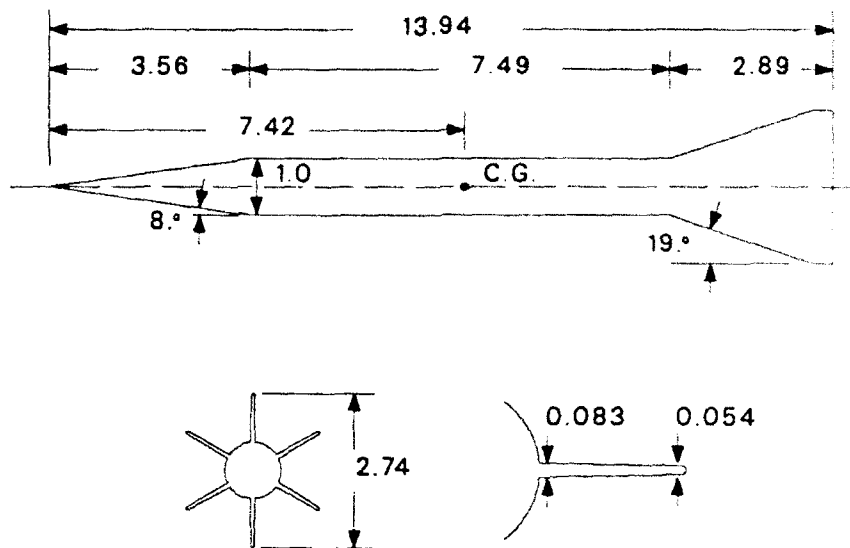
ALL DIMENSIONS IN CALIBERS (ONE CALIBER = 35.2 mm)

Figure 5. Schematic of M735 projectile.

LEADING EDGE   TRAILING EDGE
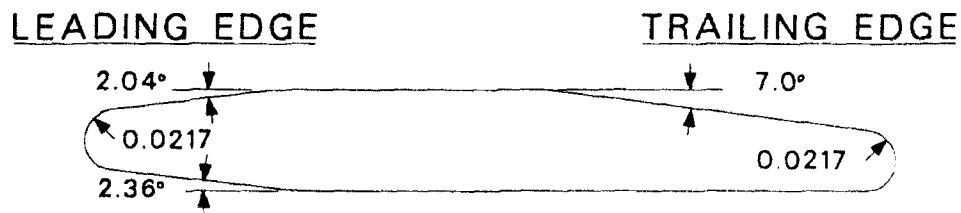
ALL DIMENSIONS IN CALIBERS (ONE CALIBER = 35.2 mm)

Figure 6. Schematic of M735 fin cross-section.
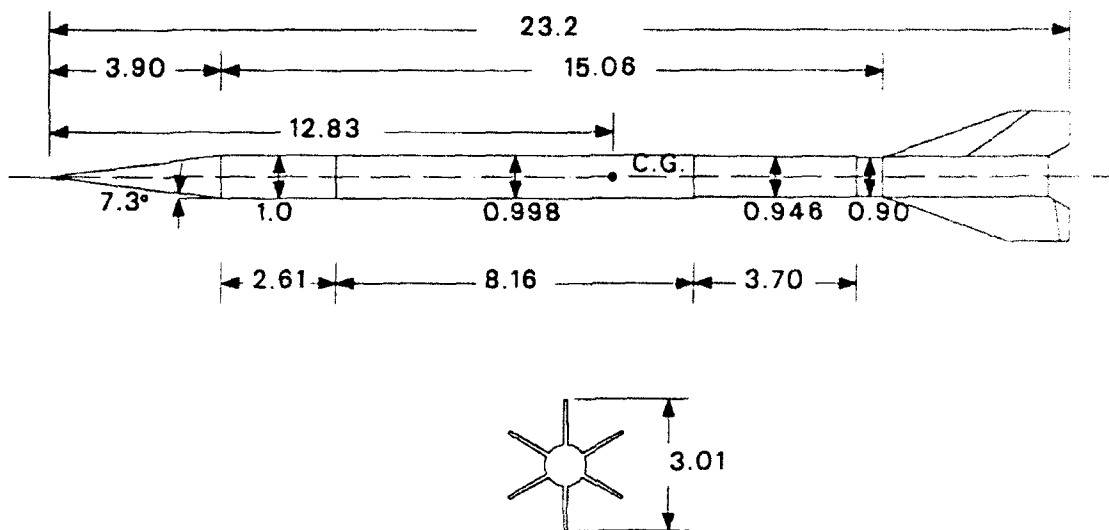
ALL DIMENSIONS IN CALIBERS (ONE CALIBER = 27.05 mm)

Figure 7. Schematic of M829 projectile.
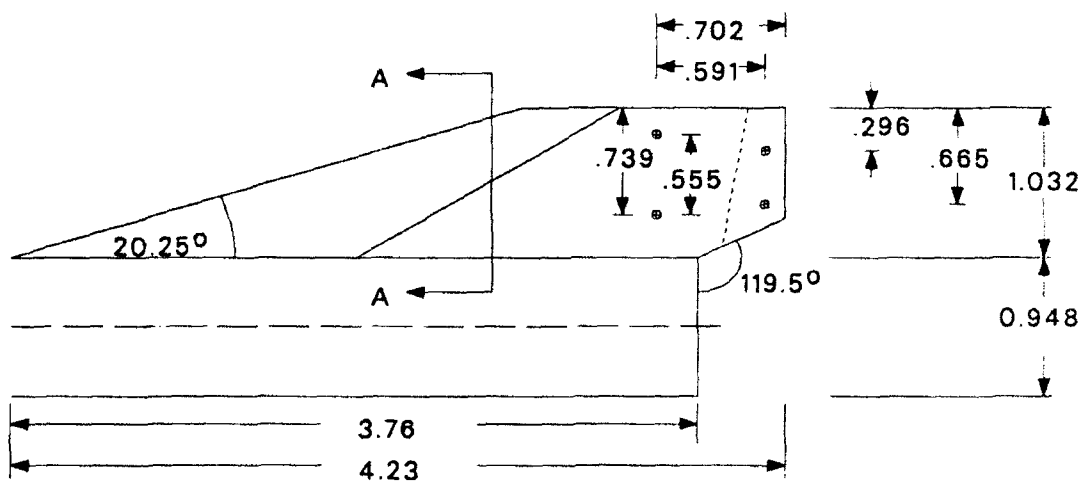
ALL DIMENSIONS IN CALIBERS (ONE CALIBER = 27.05 mm)

Figure 8. Schematic of M829 fin.

.0787

4.75°

.0924
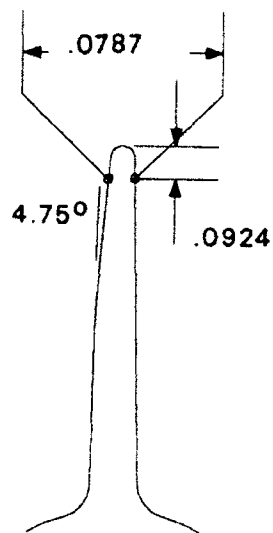
SECTION A-A

Figure 9. Detail of M829 leading edge.

.1220

.0998

.0961

.0887
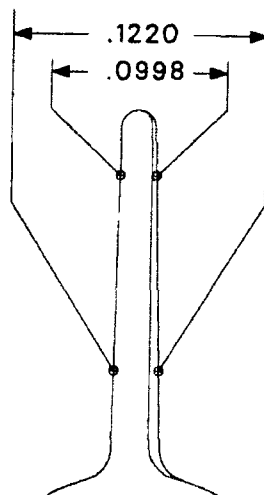
TAPERED SECTION
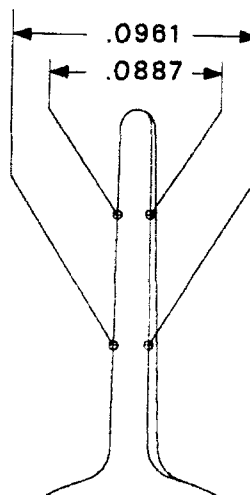
BEVELED SECTION
BEVEL ANGLE = 6.5°

Figure 10. Detail of M829 trailing edge.
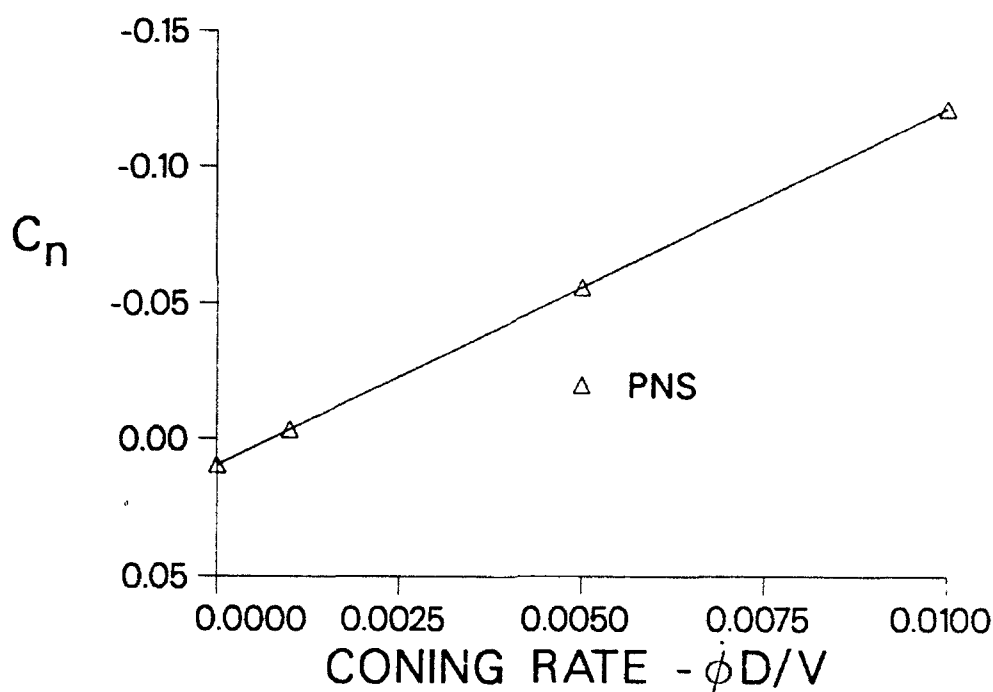
Figure 11. Variation of side moment coefficient with coning rate, M735, Mach 4, $\alpha_t = 2°$.
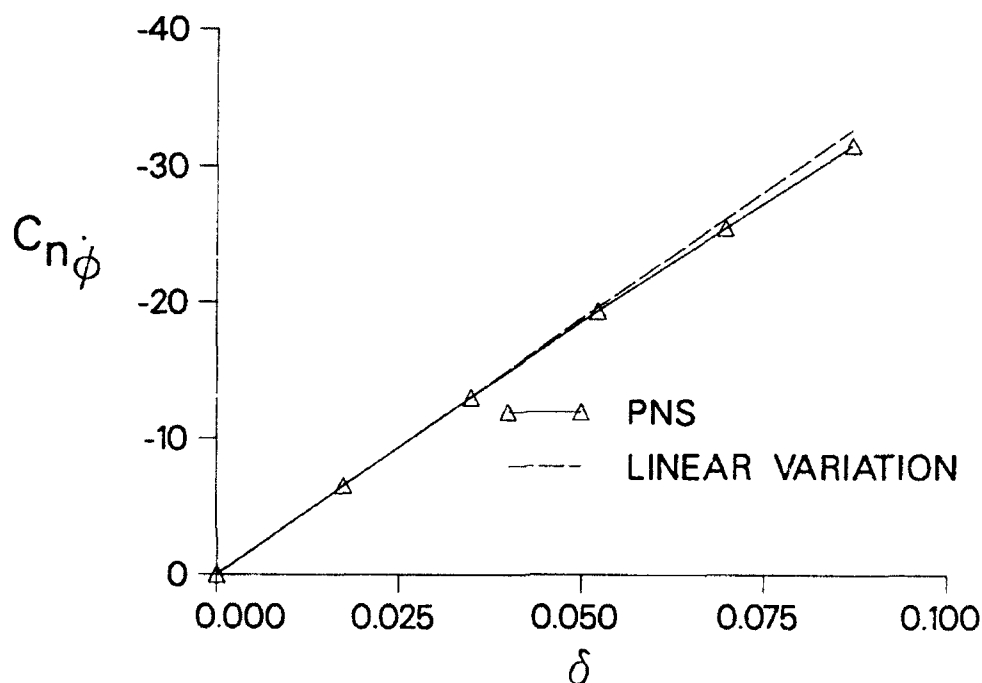
Figure 12. Side moment coefficient due to coning, $C_{n_{\dot{\phi}}}$, as a function of the sine of the angle of attack, δ, M735, Mach 4.
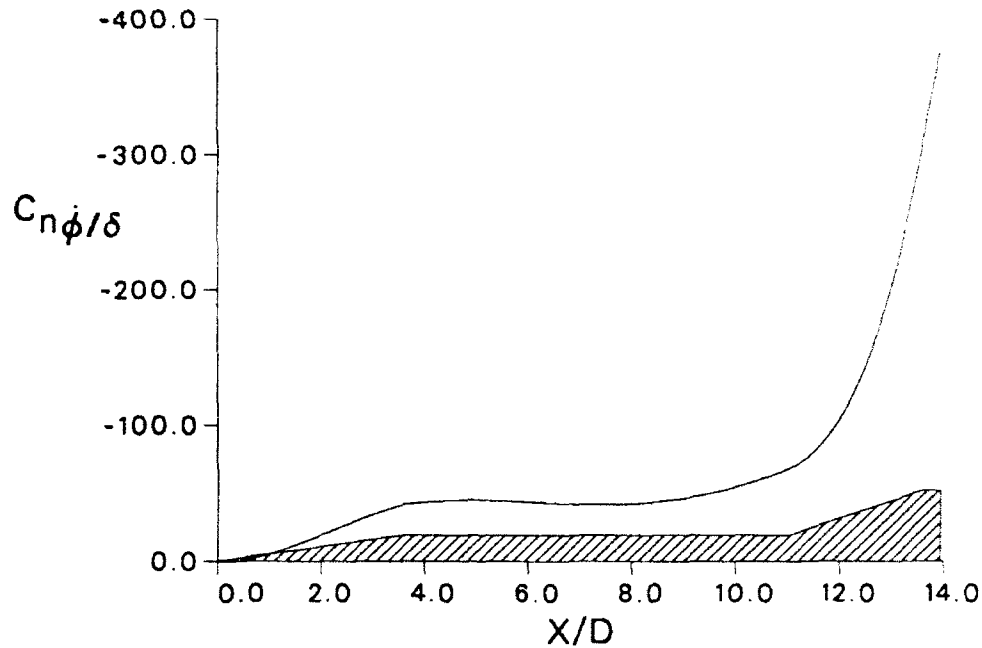
Figure 13. Development of normalized side moment slope due to coning, $\frac{C_{n_\varphi}}{\delta}$, over M735 projectile, Mach 4.
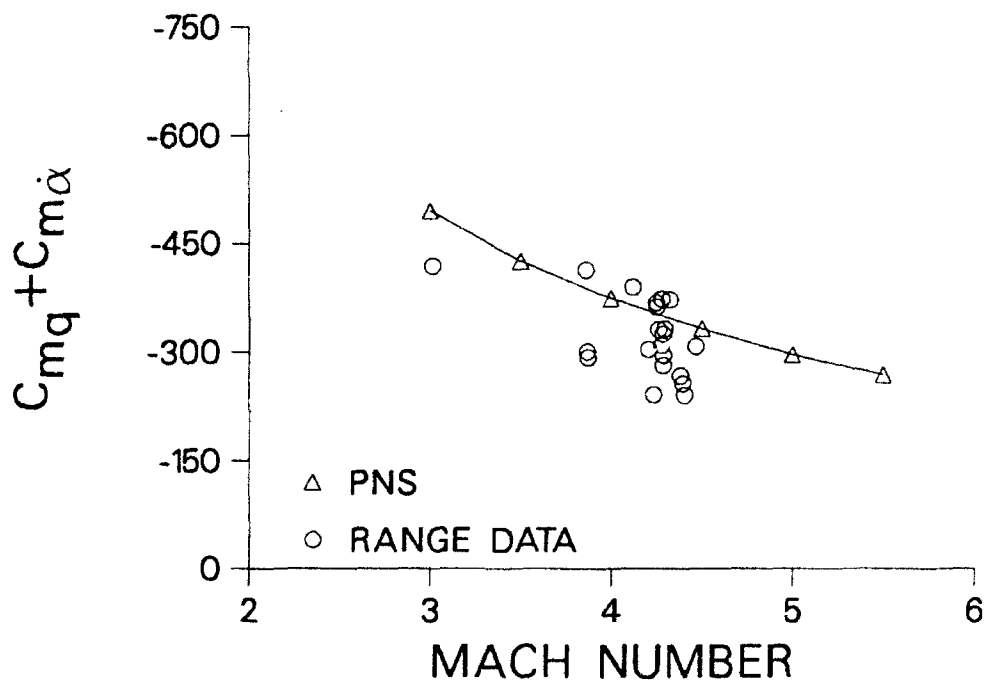
Figure 14. Mach number variation of pitch damping moment coefficient determined from side moment due to coning compared with range measurements, M735.

23
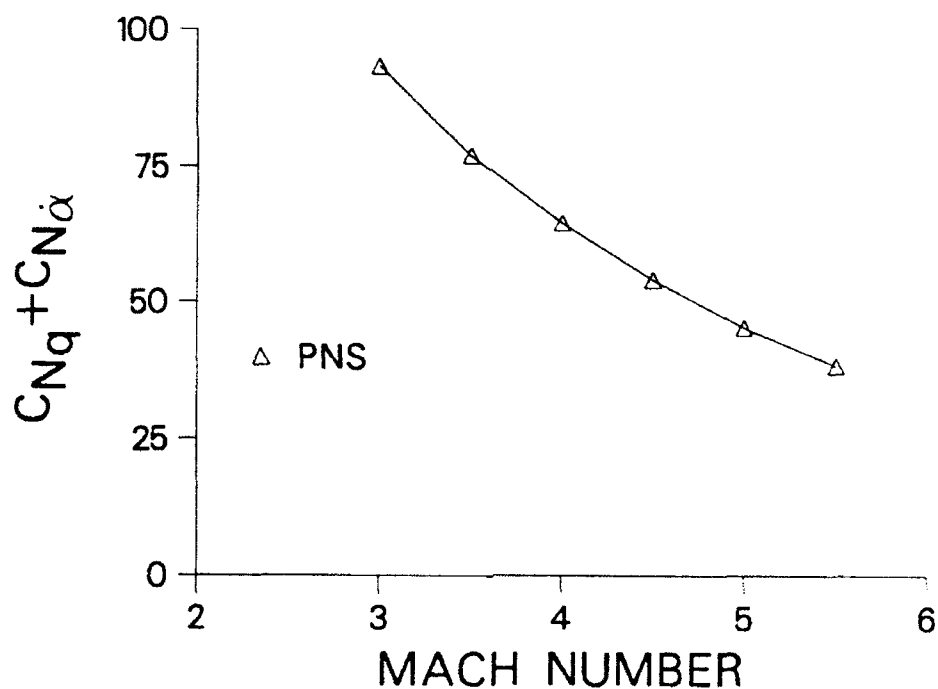
Figure 15. Mach number variation of pitch damping force coefficient as determined from side force due to coning, M735.
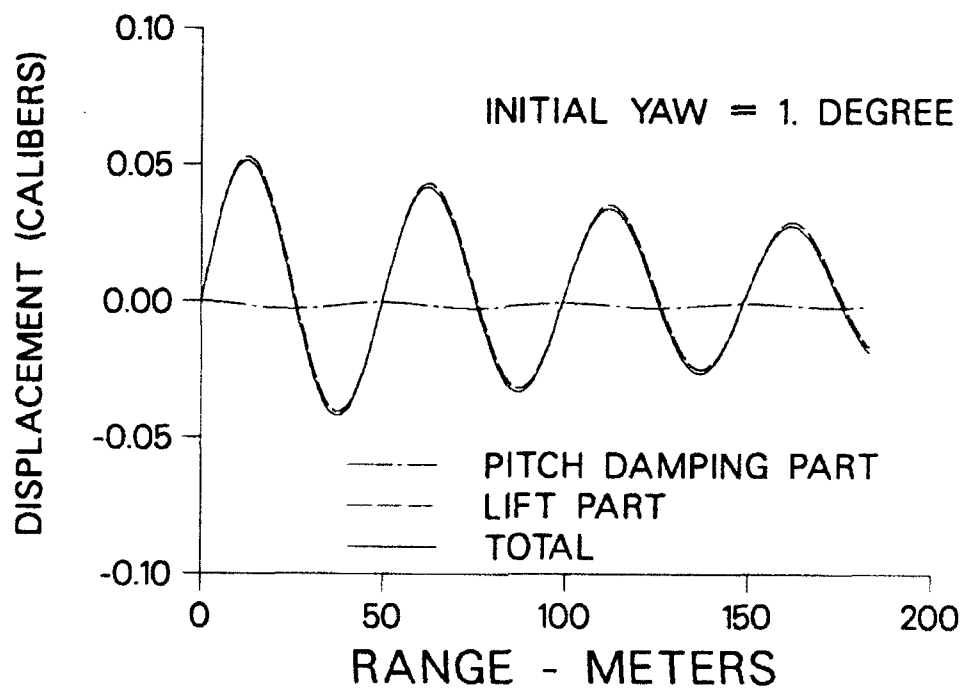
Figure 16. Fluctuating component of the swerving motion for planar pitching motion, M735, Mach 4, one degree initial yaw.
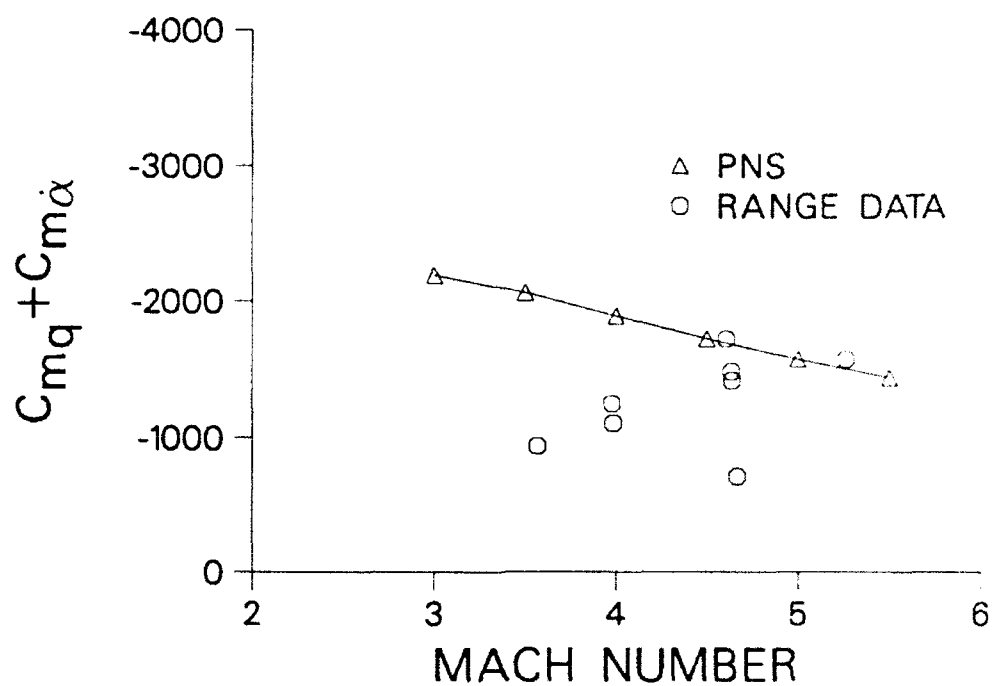
Figure 17. Mach number variation of pitch damping moment coefficient determined from side moment due to coning compared with range measurements, M829.
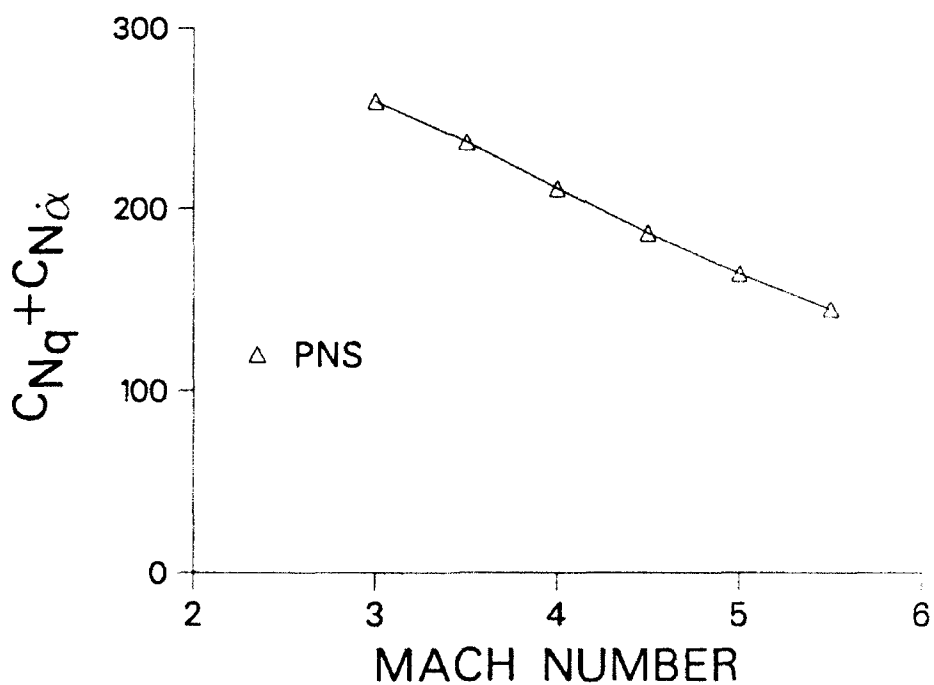
Figure 18. Mach number variation of pitch damping force coefficient as determined from side force due to coning, M829.

INTENTIONALLY LEFT BLANK.

6. REFERENCES

Agarwal, R., and J.V. Rakich. "Computation of Supersonic Laminar Viscous Flow Past a Pointed Cone at Angle of Attack in Spinning and Coning Motion." AIAA Paper 78-1211. Paper presented at the AIAA 11th Fluid and Plasma Dynamics Conference, Seattle, WA, July 1978.

Baldwin, B. S., and H. Lomax. "Thin Layer Approximation and Algebraic Model for Separated Turbulent Flows." AIAA Paper 78-257. Paper presented at the AIAA 16th Aerospace Sciences Meeting, Huntsville, AL, January, 1978.

Beam, R., and R. F. Warming. "An Implicit Factored Scheme for the Compressible Navier-Stokes Equations." AIAA Journal, vol. 16, no. 4, pp. 393-402, 1978.

Brandon, F.J. "Unpublished Ballistic Range Data," U.S. Army Ballistic Research Laboratory, Aberdeen Proving Ground, MD.

Devan, L. "Nonaxisymmetric Body, Supersonic, Inviscid Dynamic Derivative Prediction." AIAA Paper 89-2195-CP. Paper presented at the AIAA 7th Applied Aerodynamics Conference, Seattle, WA, August 1989.

Levy, L.L., and M. Tobak. "Nonlinear Aerodynamics of Bodies of Revolution in Free Flight." AIAA Journal, vol. 8, no. 12, pp. 2168-2171, December 1970.

Lin, T.C. "A Numerical Study of the Aerodynamics of a Reentry Vehicle in Steady Coning Motion." AIAA Paper 78-1358. Paper presented at the AIAA Atmospheric Flight Mechanics Conference, Palo Alto, CA, August 1978.

Murphy, C.H. "Free Flight Motion of Symmetric Missiles." Report No. 1216. U.S. Army Ballistic Research Laboratory, Aberdeen Proving Ground, MD, July 1963. (AD A442757)

Rai, M. M., and D. S. Chaussee. "New Implicit Boundary Procedure: Theory and Applications." AIAA Paper 83-0123. Paper presented at the AIAA 23rd Aerospace Sciences Meeting, Reno, Nevada, January 1983.

Rai, M.M., D.S. Chaussee, and Y.M. Rizk. "Calculation of Viscous Supersonic Flows over Finned Bodies." AIAA Paper 83-1667. Paper presented at the AIAA Applied Aerodynamics Conference, Danvers, MA, July 1983.

Roecker, E., and C. Grabarek. "The Effect of Yaw and Pitch on Long Rod Penetration into Rolled Homogeneous Armor at Various Obliquities." Proceedings of the 9th International Symposium on Ballistics, vol. 2, pp. 467-473, Shrivenham, England, May 1986.

Schiff, L.B. "Nonlinear Aerodynamics of Bodies in Coning Motion." AIAA Journal, vol. 10, no. 11, pp. 1517-1522, November 1972.

Schiff, L. B., and J. L. Steger. "Numerical Simulation of Steady Supersonic Viscous Flow." AIAA Journal, vol. 18, no. 12, pp. 1421-1430, December 1980.

Schiff, L.B., and M. Tobak. "Results from a New Wind-Tunnel Apparatus for Studying Coning and Spinning Motions of Bodies of Revolution." AIAA Journal, vol. 8, no. 11, pp. 1953-1957, November 1970.

Tobak, M., and Schiff, L.B., "Generalized Formulation of Nonlinear Pitch-Yaw-Roll Coupling: Part I - Nonaxisymmetric Bodies." <u>AIAA Journal</u>, vol. 13, no. 3, pp. 323-326, March 1975.

Tobak, M., and Schiff, L.B., "Generalized Formulation of Nonlinear Pitch-Yaw-Roll Coupling: Part II - Nonlinear Coning Rate." <u>AIAA Journal</u>, vol. 13, no. 3, pp. 327-332, March 1975.

Tobak, M., L.B. Schiff, and V.L. Peterson. "Aerodynamics of Bodies of Revolution in Coning Motion." <u>AIAA Journal</u>, vol. 7, no. 1, pp. 95-99, January 1969.

Weinacht, P., and W.B. Sturek. "Navier-Stokes Predictions of Static and Dynamic Aerodynamic Derivatives for High L/D Finned Projectiles." <u>AGARD Conference Proceedings No. 493, Missile Aerodynamics</u>, pp. 20-1:20-12, Friedrichshafen, Germany, April 1990.

LIST OF SYMBOLS

a	speed of sound
C_m	pitching moment coefficient
C_{m_α}	slope of the pitching moment coefficient with angle of attack
$C_{m_q} + C_{m_\alpha}$	pitch damping moment coefficient
C_n	side moment coefficient
C_{n_α}	slope of the side moment coefficient with angle of attack
$C_{n_{\dot\phi}}$	slope of the side moment coefficient with coning rate
$C_{n_{p\alpha}}$	Magnus moment coefficient
C_{N_α}	slope of the normal force coefficient with angle of attack
$C_{N_q} + C_{N_\alpha}$	pitch damping force coefficient
$C_{Y_{\dot\phi}}$	slope of the side force coefficient with coning rate
$C_{Y_{p\alpha}}$	Magnus force coefficient
D	projectile diameter
$\tilde{D}$	Jacobian matrix of the source term, $\hat{H}$
e	total energy per unit volume, non-dimensionalized by $\rho_\infty a_\infty^2$
$\hat{E}, \hat{F}, \hat{G}$	flux vectors in transformed coordinates
$\hat{H}$	source term resulting from rotating coordinate frame
J	Jacobian
l	characteristic length, typically the projectile diameter
M_∞	freestream Mach number
p	pressure, as used in thin-layer Navier-Stokes equations, non-dimensionalized by $\rho_\infty a_\infty^2$
p	spin rate, as used in roll equations and aerodynamic coefficients
Pr	Prandtl number
Pr_t	turbulent Prandtl number
q	vector of dependent variables in Navier-Stokes equations
q	total velocity of fluid
Re	Reynolds number, $a_\infty \rho_\infty D / \mu_\infty$
s	distance downrange
s_{cg}	center of gravity shift, calibers
$\hat{S}$	viscous flux vector in transformed coordinates
S_{ref}	reference cross sectional area of projectile, $\pi D^2 / 4$
t	time
u, v, w	velocity components in x, y, and z directions, non-dimensionalized by a_∞
U, V, W	Contravariant velocities of the transformed Navier-Stokes equations
V	freestream velocity used to non-dimensionalize the spin rate and the aerodynamic coefficients
x, y, z	Cartesian coordinates with respect to the body, non-dimensionalized by D
x_{cg}	axial location of projectile center of gravity with respect to Cartesian coordinate system

Greek Symbols

α	vertical component of total angle of attack in non-rolling coordinates
α_t	total angle of attack, $\sqrt{\alpha^2 + \beta^2}$
β	horizontal component of total angle of attack in non-rolling coordinates
γ	ratio of specific heats, as used in Navier-Stokes equations
γ	cosine of the angle of attack, as used in aerodynamic force and moment formulations
δ	sine of the total angle of attack
μ	laminar viscosity
μ_t	effective turbulent viscosity
ξ, η, ζ	transformed coordinates in Navier-Stokes equations
$\tilde{\xi}$	complex quantity representing the components of the sine of the angle of attack with respect to the non-rolling coordinate frame
ρ	density
$\dot{\phi}$	coning rate of projectile
$\frac{\dot{\phi}D}{V}$	non-dimensional coning rate
Ω_c	coning rate of projectile, non-dimensionalized by a_∞/D

Superscripts

$(\dot{\ })$	rate of change with respect to time
$(\ )'$	rate of change with respect to space
$(\tilde{\ })$	quantity is referenced to the non-rolling coordinate frame

Subscripts

∞	freestream quantity

31

No. of Copies	Organization	No. of Copies	Organization
2	Institute of Advanced Technology University of Texas, Austin ATTN: Dr. T. Kiehne Dr. W. G. Reineke 4030-2 W. Braker Lane Austin, TX 78759-5329	1	General Research Corporation ATTN: Dr. Hartley King 5383 Hollister Ave. P.O. Box 6770 Santa Barbara, CA 93160-6770
2	Alliant Techsystems, Inc. ATTN: Mark W. Swenson Richard J. Buretta Mail Station MN48-3700 7225 Northland Drive Brooklyn Park, MN 55428	1	Science and Technology Associates, Inc. ATTN: Mr. Bruce Lohman 4001 North Fairfax, Suite 700 Arlington, VA 22203-1618
1	Arrow Technology Associates ATTN: Robert Whyte P.O. Box 4218 Burlington, VT 05491-0042		
1	McDonnell Douglas Corporation ATTN: Dr. Thomas P. Gielda Dept. 222, Bldg 110, Lev 1 RM/PT 151 Mail Code 5 P.O. Box 516 St. Louis, MO 63166-0516		

4	General Electric Aerospace
	ATTN: Dr. James E. Daywitt
	        Mr. Yick Chan
	        Dr. David Szostowski
	        Dr. Robert Brewer
	Bldg 100-VFSC, Room U-4019
	230 Goddard Blvd.
	King of Prussia, PA 19406		

2	VRA, Inc. ATTN: Dr. C. Lewis Dr. B. A. Bhutta P.O. Box 50 Blacksburg, VA 24060		
1	McDonnell Douglas Missile Systems Co. ATTN: F. McCotter Mail Code 306-4249 P.O. Box 516 St. Louis, MO 63166-0516		

INTENTIONALLY LEFT BLANK.

USER EVALUATION SHEET/CHANGE OF ADDRESS

This Laboratory undertakes a continuing effort to improve the quality of the reports it publishes. Your comments/answers to the items/questions below will aid us in our efforts.

1. ARL Report Number ___ARL-TR-112___ Date of Report ___April 1993___

2. Date Report Received _____

3. Does this report satisfy a need? (Comment on purpose, related project, or other area of interest for which the report will be used.) _____

_____

_____

4. Specifically, how is the report being used? (Information source, design data, procedure, source of ideas, etc.) _____

_____

_____

5. Has the information in this report led to any quantitative savings as far as man-hours or dollars saved, operating costs avoided, or efficiencies achieved, etc? If so, please elaborate. _____

_____

_____

6. General Comments. What do you think should be changed to improve future reports? (Indicate changes to organization, technical content, format, etc.) _____

_____

_____

_____

	Organization
CURRENT ADDRESS	Name
	Street or P.O. Box No.
	City, State, Zip Code

7. If indicating a Change of Address or Address Correction, please provide the Current or Correct address above and the Old or Incorrect address below.

	Organization
OLD ADDRESS	Name
	Street or P.O. Box No.
	City, State, Zip Code

(Remove this sheet, fold as indicated, tape closed, and mail.)
(DO NOT STAPLE)

DEPARTMENT OF THE ARMY

OFFICIAL BUSINESS

BUSINESS REPLY MAIL
FIRST CLASS PERMIT No 0001, APG, MD

Postage will be paid by addressee

Director
U.S. Army Research Laboratory
ATTN: AMSRL-OP-CI-B (Tech Lib)
Aberdeen Proving Ground, MD 21005-5066

NO POSTAGE
NECESSARY
IF MAILED
IN THE
UNITED STATES